Wang *et al.*
European Journal of Medical Research (2024) 29:608
https://doi.org/10.1186/s40001-024-02194-8

European Journal of Medical Research

RESEARCH

Open Access

The role of m6A methylation genes in predicting poor prognosis in sepsis: identifying key biomarkers and therapeutic targets

Shaokang Wang[1], Siye Shen[1], Na Cheng[2], Wenjun Zhou[1], Weili Yu[1], Daiyun Liang[1], Lijun Cao[1], Pinjie Zhang[1], Zhonghua Lu[1*] and Yun Sun[1*]

Abstract

Sepsis is one of the leading causes of death among seriously ill patients worldwide, affecting more than 30 million people annually and accounting for 1–2% of hospitalizations. By analyzing gene expression omnibus (GEO) data set, our team explored the relationship between m6A methylation gene and poor prognosis of sepsis. The purpose of this present study is to examine new detection markers for patients with poor prognosis, provide theoretical basis for timely intervention and improve the survival rate of patients. First, GSE54514 transcriptome data were extracted from the GEO database 31 patients with sepsis related death and 72 sepsis survivors. Key genes were screened from differentially expressed genes (DEGs), least absolute shrinkage and selection operator (LSAAO) and random forest (RF). And then, METTL3, WTAP and RBM15 were further verified by quantitative reverse transcription PCR (qRT-PCR). The constructed nomogram model showed high accuracy in predicting death. These three genes are mainly involved in chemokine signaling pathway, differentiation of monocytes and *T* cells, and phagocytosis of immune cells. The analysis showed that a high m6A score subtype is linked to lower immunosuppression and higher survival rates in clinical samples, suggesting better immune responses and outcomes for these patients. Finally, the protective effect of METTL3 in sepsis was demonstrated in mouse sepsis model applied with METTL3 inhibitor, by conducting cell flow cytometry analysis, enzyme-linked immunosorbent assay (ELISA) and hematoxylin–eosin (HE) staining. In conclusion, these findings provide potential biomarkers and targets for early precision diagnosis and treatment.

Keywords Sepsis, GEO, QRT-PCR, METTL3

Introduction

Sepsis is an infection-triggered, critical immune system disease usually accompanied with life-threatening organ impairment [1, 2]. Despite the rapid advances in medical procedures, sepsis remains a major clinical challenge in the field of acute and critical care medicine [3]. A meta-analysis involving 51 studies showed that there were 189 cases of sepsis per 100,000 person-years, with a mortality rate of 26.7%. In the ICU setting, the incidence rate was 58 per 100,000 person-years, with a higher mortality rate of 41.9% [4]. The annual medical expenses caused

*Correspondence:
Zhonghua Lu
luzhonghua@ahmu.edu.cn
Yun Sun
sunyun9653@126.com
[1] The Second Affiliated Hospital of Anhui Medical University, 678 Furong Road, Hefei 230601, Anhui Province, China
[2] School of Biomedical Engineering, Anhui Medical University, 81 Meishan Road, Hefei 230032, Anhui Province, China

by sepsis amount to billions of dollars each year, imposing a heavy economic burden on families and society. In addition, the high morbidity and mortality rates of sepsis increases the pressure on medical resources, especially in developing countries where inadequate medical facilities and a shortage of medical staff pose greater challenges to the treatment and management of patients with sepsis [5]. Early recognition and appropriate treatment can significantly improve outcome of sepsis patients. With the in-depth understanding of the pathogenesis of sepsis and the advancement of diagnostic technology, individual or group physiological parameters have been used to predict severe complications. Therefore, screening survival genes associated with sepsis, studying different subtypes of sepsis, and clarifying its causes are all effective means to reduce the risk of death in patients with sepsis and may provide new directions for clinical treatment.

In recent years, epigenetic modification mechanisms have gradually shown a central role in controlling disease progression. Methylation modification of N6-methyladenosine (m6A) is a common means of biofunctional modification in organisms, and several studies have revealed key mechanisms related to the occurrence and development of sepsis [6]. This means of biomodification of m6A is associated with several biological processes such as RNA shearing, translocation, translation, and degradation [7]. Furthermore, m6A modification is reversible and consists of methylase (writer), demethylase (eraser), and methyl-recognition proteins (reader), and is dynamically tuned by the interaction between these functions [8]. Recent researches indicated that m6A methylation plays a crucial role in the occurrence and development of various diseases [6]. It was reported that METTL3-mediated m6A modification could promote the stabilization of PD-L1 mRNA in an IGF2BP3-associated manner in breast cancer cells and maybe positively correlated with tumor immunotherapy [9]. Besides, in neurodegenerative diseases such as Alzheimer's and Parkinson's, m6A modification was also indicated to play an important role in maintaining the survival and function of neurons [10]. Furthermore, in autoimmune diseases like rheumatoid arthritis (RA), m6A methylation regulators could be used to predict RA diagnosis and might additionally regulate the inflammatory activity [11]. In summary, m6A methylation is closely associated with cell survival and inflammatory process.

Given its significance in cancer, neurological diseases, and immune diseases, the potential character of m6A methylation and modulators in the diagnosis, therapeutics, and prognosis of sepsis attracts more attention. Studies have shown that m6A modification plays a key pathophysiological role in sepsis-induced organ dysfunction, such as heart failure, acute lung injury (ALI), and acute kidney injury (AKI), and is sometimes even used as a therapeutic target [12]. By using a CLP-induced sepsis-associated ALI mouse model, Zhang et al. reported a critical role of METTL3 in sepsis-induced ALI pathogenesis through Neutrophil extracellular traps-mediated m6A modification of alveolar epithelial cells [13]. In another sepsis induced cardiomyopathy in CLP mouse model, researchers found that M6A modification plays an indispensable regulatory role in cardiomyocyte apoptosis and inflammatory activity [14]. The studies on the m6A regulators in sepsis remains limited and the underlying mechanisms are still unrevealed.

Public databases provide us with rich transcriptomic data related to sepsis, which helps us to better understand the potential impact of sepsis-associated m6A RNA methylation molecules on sepsis. In this study, we applied a bioinformatics approach to investigate the role of sepsis survival genes in the survival status and classification of sepsis patients. First, we identified the relevant data in the data set of GSE54514 and screened four genes that are closely associated with sepsis survival using support vector machine–recursive feature elimination (SVM–RFE), most LASSO, and RF algorithms. The three key genes were further screened by qRT-PCR. We then constructed a nomogram model for the three genes involved with sepsis survival for prediction of morbidity and further classified the expression profiles into three3 different categories, and also investigated the interconnections of these key genes with immune cells. Finally, we used a CLP-induced mouse sepsis model to investigate the regulatory role of METTL3-mediated m6A modification in different severity of sepsis.

Methods

Experimental design and process

The flow chart of this study is shown in Fig. 1.

Data collection and preprocessing

Microarray data sets were downloaded from the GEO database (https://www.ncbi.nlm.nih.gov/geo/), using "sepsis," "whole blood," and "Homo sapiens" as core keywords. GSE54514 was downloaded from the GEO database on the GPL570 platform, covering 30 sepsis patients and 97 fatal sepsis patients [15].

Data preprocessing

All data sets were downloaded in txt. file format, and the data from mRNA arrays were used for positive exponential background correction, followed by quantile normalization across arrays using the limma R package. Finally, we excluded healthy patients from the data set, retaining only the survival and death gene expression matrices of sepsis patients.

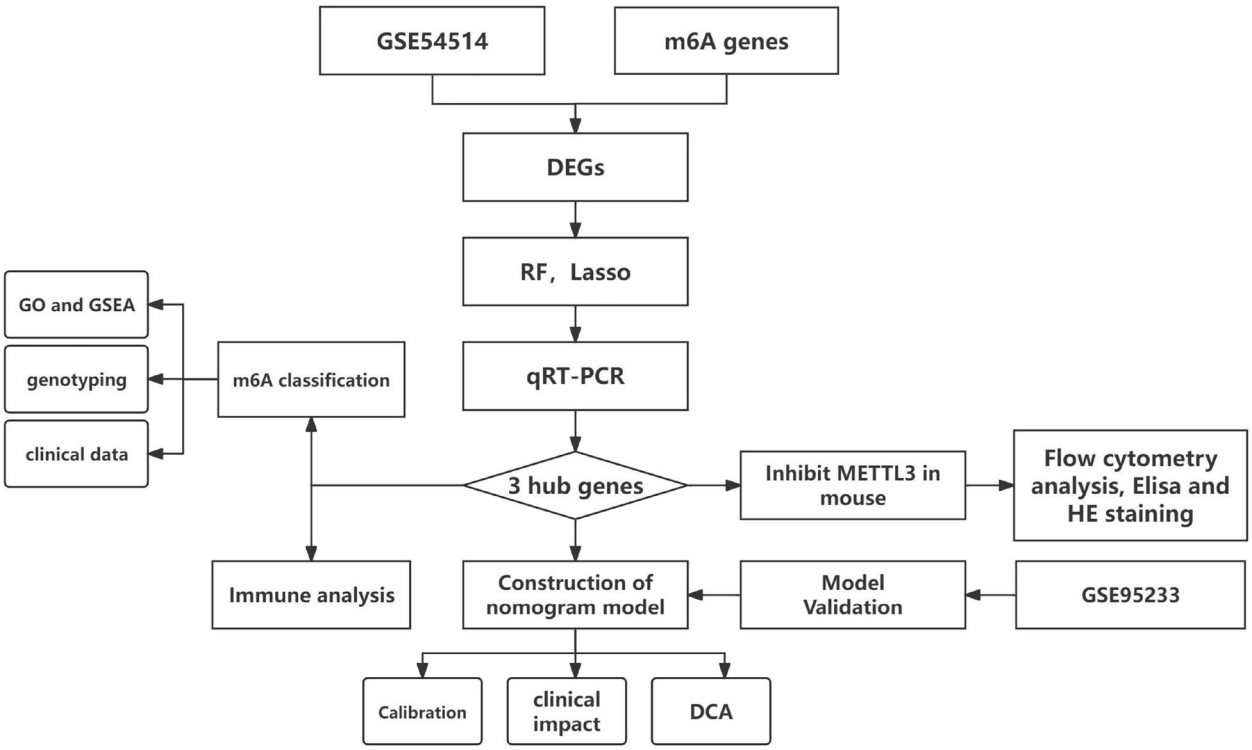

Fig. 1 Overall design flow chart of the bioinformatic analysis and validation

Identification of hub genes in sepsis

We standardized the GSE54514 cohort using the "limma" package in R. Based on prior literature, we identified 26 m6A regulatory factors [16], but only 24 were present in the data set after intersection with GSE54514. We visualized differential expression using "pheatmap" and "ggpubr" to generate heatmaps and box plots. Three feature selection algorithms—SVM–RFE [17], LASSO logistic regression [18], and RF algorithm [19]—were used to screen sepsis survival-related biomarkers. The RF algorithm was analyzed with "randomForest" [20], and LASSO logistic regression with "glmnet" [21]. Genes from these algorithms were considered as sepsis characteristic genes for further analysis.

Validation and screening by qRT-PCR

1. Study subjects: Blood samples collected on the first day of diagnosis from sepsis patients admitted to the Second Affiliated Hospital of Anhui Medical University between October 1, 2023, and December 31, 2023, who met the diagnostic criteria of the "2021 International Guidelines for Management of Sepsis and Septic Shock" record whether the patient survived.
2. Study methods: 1. Sample processing: Total RNA was extracted from previously stored blood samples using the Trizol reagent kit. 2. qRT-PCR validation: The expression levels of METTL3, METTL14, WTAP, and RBM15 were detected using specific primers and probes with the qRT-PCR technique. GAPDH was used as the internal reference gene.

Establishment of prognostic model

We used the "rms" package in R to create a nomogram model [22]. The predictive accuracy and maximum benefit level of the model were assessed using calibration curves, clinical decision curves (DCA), and clinical impact curves (CIC) [23]. The accuracy and generalizability of the model were validated in an independent cohort by calculating its AUC value.

m6A subtyping and evaluation of sepsis

Consensus clustering algorithms identify and classify each member in a data set [24]. To determine the optimal number of clusters, we used the CDF curve of consensus scores, clear distinctions in consensus matrix heatmaps, characteristics of the consensus cumulative distribution function plots, and ensured sufficient matching

consistency among cluster members [25]. We employed PCA to calculate sepsis sample scores.

Immune cell infiltration

Single sample gene set enrichment analysis (ssGSEA) was conducted using the R packages "limma," "GSVA," and "GSEABase" to determine the relative abundance of immune cells in sepsis with different outcomes [26]. The gene sets marking each type of immune cell were obtained from the study by Charoentong [27].

Animal experiments

Experimental grouping: We selected METTL3, which showed the largest differential expression among immune cells across different subtypes of the three regulatory factors, for validation. Fifteen mice were divided into three groups: normal control group (normal), sepsis model group (CLP), and intraperitoneal injection of STM2457 + sepsis model group (CLP + STM2457). Flow cytometry, enzyme-linked immunosorbent assay (ELISA), and HE staining were used to evaluate pro-inflammatory cytokines in mouse lung tissue.

Treatment of groups: The CLP + STM2457 group received daily intraperitoneal injections of STM2457 (50 mg/kg) for 3 days, while the other two groups were injected with an equal volume of saline. After 3 days of injections, mice requiring sepsis modeling underwent cecal ligation and puncture (CLP), while the control group had a laparotomy without further intervention. 24 h after model establishment, tissue samples were collected.

Flow cytometry: Cells were isolated from spleen tissue by grinding and filtering, followed by red blood cell lysis. After diluting to a concentration of 1 × 10^6 cells/100 μL, they were incubated with anti-CD16/CD32 antibody at 4 °C for 15 min to block Fc receptors. The cells were then washed twice with ice-cold PBS (pH 7.2) containing 0.1% NaN3 and 0.5% BSA. Subsequently, the cells were incubated with fluorescent antibodies at 4 °C for 30 min, washed twice, and resuspended in 300 μL of PBS. The fluorescent antibodies used included: PE-conjugated anti-mouse IL-17A, BV421-conjugated anti-mouse CD4, PerCP-Cy™5.5-conjugated anti-mouse CD45, and APC-conjugated anti-mouse IFN-γ. The stained cells were analyzed using a Beckman CytoFLEX flow cytometer. White blood cell populations were identified using CD45 labeling (CD45 +). CD4 + T cells (CD45 + CD4 +) were selected based on CD4 expression. Th1 and Th17 subsets were distinguished by staining for IFN-γ and IL-17A, identifying Th1 cells (CD45 + CD4 + IFN-γ +) and Th17 cells (CD45 + CD4 + IL-17A +). Data acquisition was performed using CytExpert software (Beckman Coulter, version 2.4), followed by analysis to assess specific immune cell infiltration.

ELISA: Blood was collected from the orbital area and then centrifuged to obtain serum. The levels of IL-6 (ELK Biotechnology #ELK1157), IL-1β (ELK Biotechnology #ELK1271), TNF-α (ELK Biotechnology #ELK1387) were determined according to the ELISA kit instructions.

HE staining: In brief, these tissues of lungs, liver, kidneys, and small intestine were fixed with formalin, embedded in paraffin, sectioned and observed under a 40 × light microscope. Previous studies have introduced criteria for evaluating tissues pathological changes [28–32].

Statistical analysis

Statistical analysis was performed using SPSS 21 and GraphPad Prism 7 software. A *P* value less than 0.05 was considered statistically significant.

Results

m6A genes related to sepsis were screened First

We performed sample screening on the data expression matrix of GSE54514 and excluded normal patient samples, retaining only patient samples with sepsis survival and death outcomes. We then compared these samples with 26 m6A methylated genes from the literature and finally identified 24 m6A methylated genes and their expression. Next, we used machine learning algorithms of RF and Support Vector Machine (SVM) on the screened transcriptome data. We selected the expressions of 24 m6A methylated genes as independent variables and included the processed data sets sepsis survival group and sepsis death group as outcome variables in the RF and SVM models, respectively. We analyzed the frame plots and cumulative residual distributions of the two models to determine which model performed better. The RF had lower mean residual values compared to the SVM (Fig. 2a), whereas the inverse cumulative distribution line of residuals for the RF was located predominantly within the residual line of the SVM (Fig. 2b). In addition, the AUC value of RF reaches 1.000, which is higher than the 0.955 of SVM (Fig. 2c), which means that the gap between the predicted and actual values of RF is relatively small, thus proving that the model is more accurate. Therefore, we decided to use the RF model to predict m6A genes associated with sepsis.

Screening for hub genes

We screened 24 genes using difference-in-difference analysis and found significant differences in the expression of METTL3, METTL14, WTAP, RBM15, IGFBP1, and ALKBH5 between sepsis survival and death groups by box-and-line plot. By RF modeling, we further

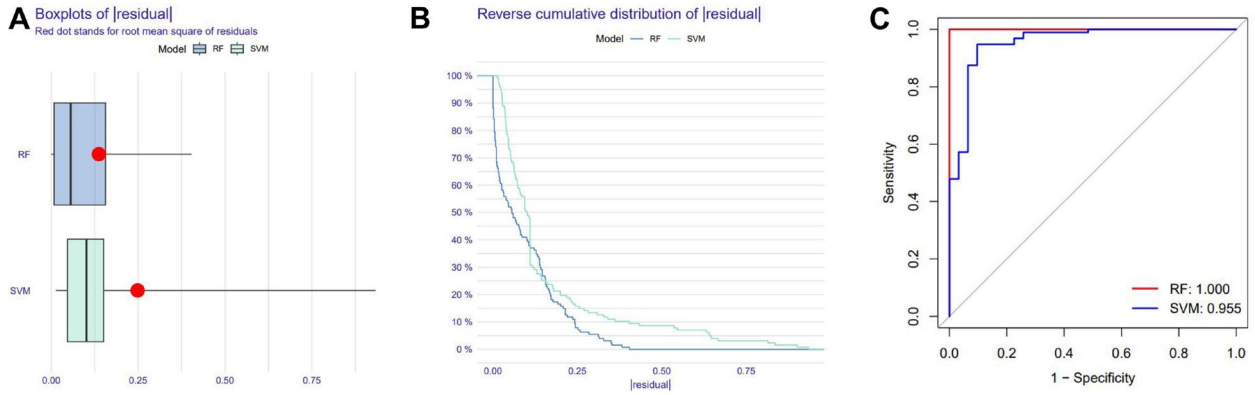

Fig. 2 Selection of models. **A** Residual box diagram, observe the residual values of RF and SMV models; **B** inverse cumulative distribution of residuals of RF and SMV; **C** comparison of ROC curves between RF and SMV

determined the importance score of sepsis-related m6A genes. A higher score implies a higher importance of the gene in the disease, and we found that the top 6 scoring genes screened by RF modeling were consistent with the results derived from differential analysis (Fig. 3c). To screen different characteristic genes related to sepsis in more depth, we used the LASSO logistic regression method and cross-analyzed the sepsis characteristic genes screened by the Lasso and RF algorithms. Based on the analysis results of these three algorithms, we finally

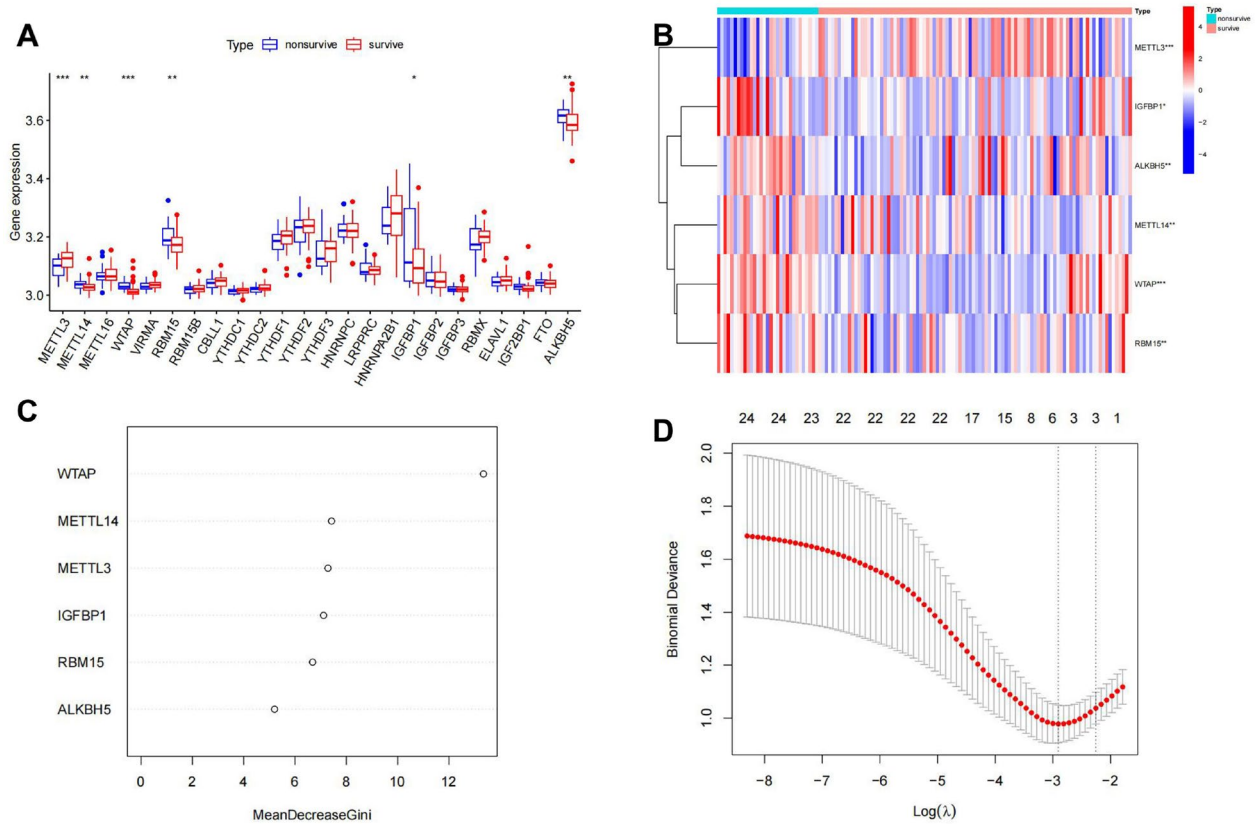

Fig. 3 Screening for sepsis survival factors: **A** Boxmaps of 26 differentially expressed genes of m6A regulators in patients who died and survived sepsis. **B**, **C** Analysis of random forest trees with differential genes. **D** LASSO regression analysis of differentially expressed genes was performed, and the genes were screened again

identified the signature genes associated with the survival of sepsis with 4 to m6A methylation.

Three genes were screened by qRT-PCR

We validated the screened four methylation regulators associated with sepsis in clinical samples. By collecting blood samples from sepsis patients with different outcomes, including samples from 20 patients with sepsis death outcome and 10 patients with sepsis survival outcome, and performing qRT-PCR for validation, we found that these 4 methylation regulators were statistically significant ($P<0.05$) in both the death and survival groups (Fig. 4). Meanwhile, we found that METTL14 was highly expressed in the sepsis survival patient group, which was inconsistent with the results of data analysis. Therefore, we finally screened out three sepsis survival-related methylation regulators, METTL3, WTAP, and RBM15.

An effective predictive model was established

We screened m6A regulators from the machine-learning-based GEO database that were significantly associated with sepsis: METTL3 WTAP RBM15. To more visually demonstrate the ability of these regulators in predicting the survival and mortality groups, we constructed a nomogram (Fig. 5a). The calibration curve (Fig. 5b) showed that the predicted sepsis risk was highly consistent with the actual observed data. In addition, we constructed a model for the prediction of clinical decision curves (Fig. 5c), and the results of the study showed that the net benefit of patients was higher when using METTL3, WTAP, and RBM15 as the characterized genes for predicting the outcome of sepsis, which indicated that the model was worth using. Finally, based on the clinical decision curve, we further drew the clinical impact curve (CIC) (Fig. 5d). The red curve (numerical high risk) is used to indicate the number of people classified as positive (high risk) by the model at each threshold probability. At each threshold probability, the blue curve (indicating the number of people at high risk with a result) represents the number of true positives. The results of the study reveal that the blue curve lies within the interval of the red curve, which proves the accuracy of the model in classification. This further confirms that METTL3, WTAP, and RBM15 can be considered as biomarkers that are significantly associated with the final outcome of sepsis. The generated model was subsequently validated using the microarray data set GSE95233. The diagnostic accuracy of the model was evaluated utilizing ROC curves as well as the area under the ROC curve (Fig. 5e, f).

Immunoassay of three sepsis survival-related genes

We assessed one of the subtypes of changes in immune status. Gene set single sample gene set enrichment analysis (ssGSEA) is an extension of GSEA to assess cellular infiltration in the sepsis microenvironment. Each GSEA ES indicates the extent to which genes are coordinately regulated upward or downward within a particular gene set. Immune cells include immune-enhancing cells (Th1, *T* cells, CD4+cells, activated NK cells, activated B cells, etc.) and immune-suppressing cells (Th2, Treg, etc.).

By comparing sepsis patients as well as immune cells, it can be seen that CD56dim NK cells and Th17 cells were highly expressed in sepsis-dead patients, whereas neutrophils, eosinophils, and macrophages were more highly expressed in sepsis-survival group (Fig. 6a); in addition, we visualized the immune cells and the three sepsis-survival genes, and it can be seen that the correlation coefficients between each gene and the corresponding correlation coefficients between each gene and the corresponding immune cells (Fig. 6b); then the genes were divided into high and low expression groups

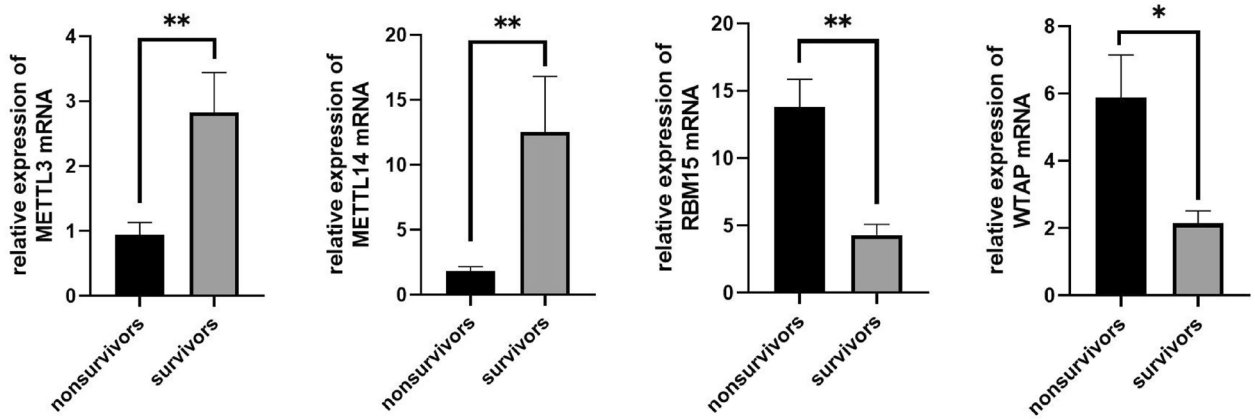

Fig. 4 Expression levels of METTL3, METTL14, WTAP and RBM15 in clinical blood samples of qRT-PCR $^{*}P<0.05$, $^{**}P<0.01$

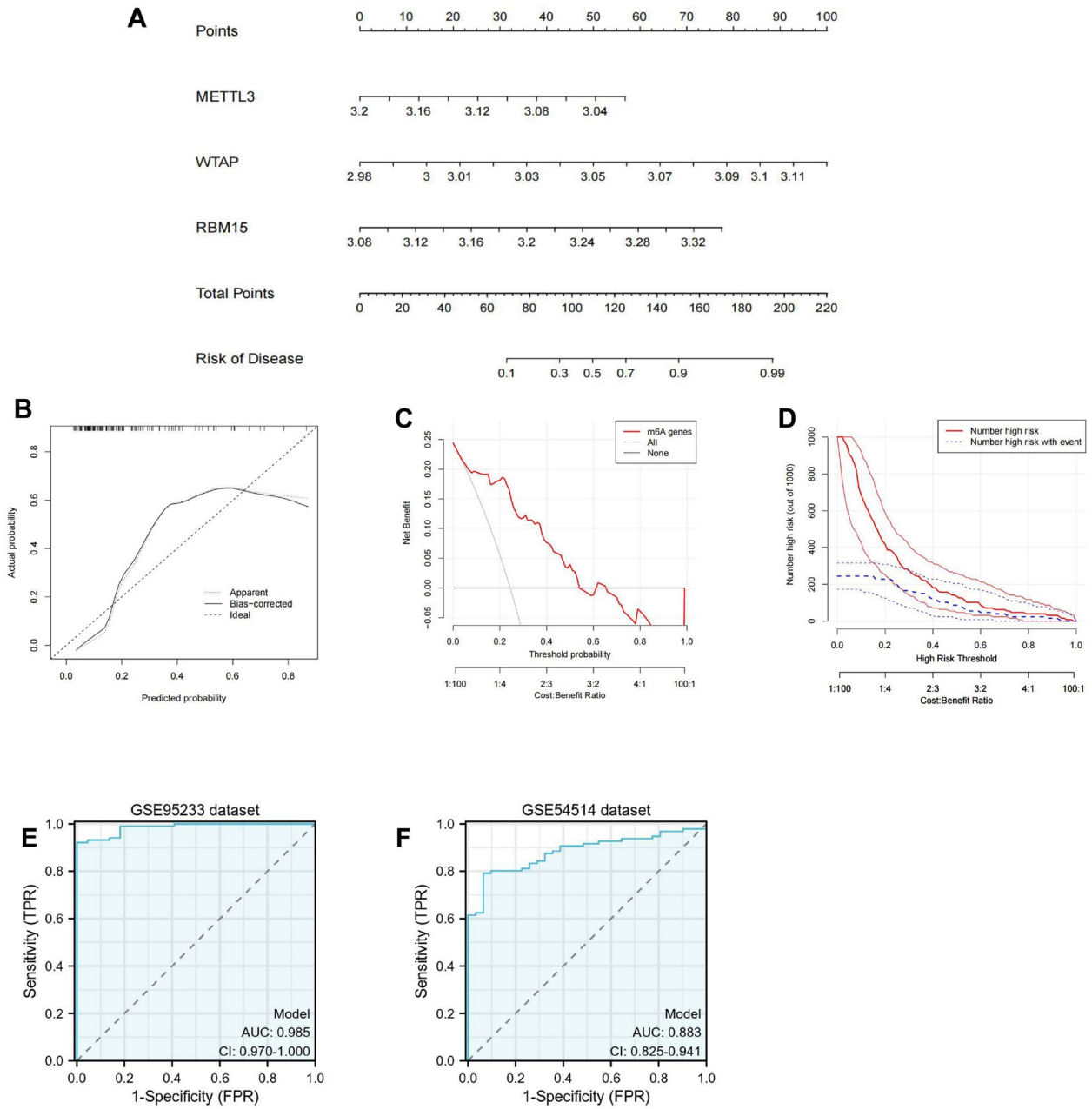

Fig. 5 Construction of nomogram model. **A** Nomogram model based on three key genes. **B** Predictive robustness of the nomogram model as shown by the correction curve. **C** Decision making based on nomogram models may benefit patients with sepsis. **D** To evaluate the clinical impact of this nomogram model through clinical impact curves. **E** The ROC curve of the nomogram in dataset GSE95233. **F** The ROC curve of the nomogram in dataset GSE54514.

according to their expression, and by comparison, we could see that more immune cells, such as Treg, Th2, Th17, etc., showed high expression levels in the high expression group of METTL3 gene; only monocytes showed differences in the expression of the WTAP gene in the high expression group; and only RBM15 low expression level group showed the expression of the DCs as well as high expression of Th17.

Identification of three different m6A subtypes in sepsis

Based on three sepsis prognosis-related genes, we employed a consensus clustering algorithm to identify

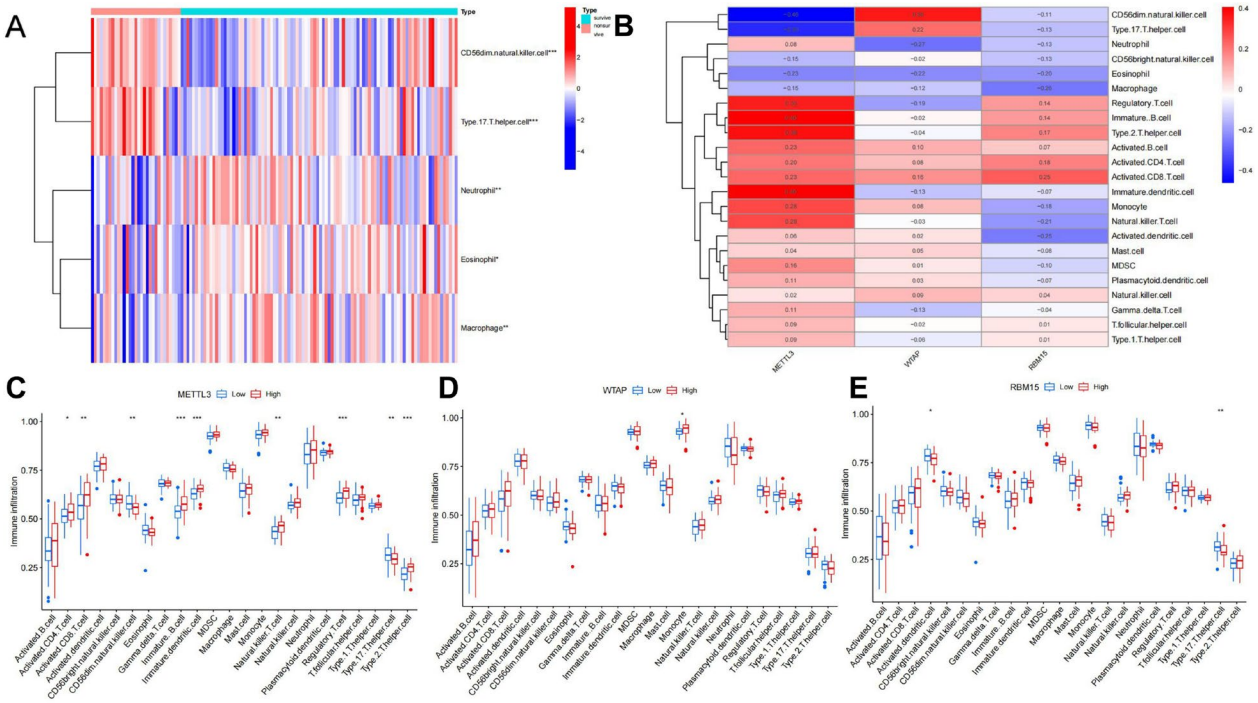

Fig. 6 Immune cell analysis: **A** Significantly different immune cells in sepsis survival group and death group. **B** Correlation between immune cells and 3 sepsis survival genes. **C**, **D**, **E** According to METTL3, WTAP, RBM15, divided into high and low expression corresponding to the expression of immune cells. * means $P<0.05$, ** means $P<0.01$, *** means $P<0.001$

different subtypes of sepsis and found that the clusters had the best stability when $k=3$, i.e., cluster A, cluster B, and cluster C. As demonstrated by the heat map of the consensus matrix, these 3 clusters presented well-defined boundaries, which meant that they exhibited excellent cluster stability during successive iterations (Fig. 7a). Next, to further confirm the accuracy of the typing, we performed a component analysis (PCA) (Fig. 7b) and performed a difference analysis for the three different subtypes (Fig. 7c), which demonstrated that there were statistically significant differences in the expression of all three genes in this classification. In addition, based on the m6A classification of sepsis, our analysis of it in combination with immune cells yielded large differences in the expression of immune cells such as CD56dim NK cells, Treg, Th17 and Th2 (Fig. 7d). More differentially expressed immune cells appeared in these subtypes, so we hypothesized that patients with sepsis under such different subtypes had large differences in immune function.

Identification of three m6A typing differential genes and functional enrichment pathways

To investigate the potential biological activities of the m6A-related isoforms, we identified 821 m6A isoform-associated DEGs among the three isoforms (Fig. 8a), followed by functional analyses to reveal the biological roles of the DEGs using the "GSEA" software. Kyoto Encyclopedia of Genes and Genomes (KEGG) analysis showed that the DEGs were mainly enriched in chemokine signaling pathways (Fig. 8b). In the biological process (BP) category (Fig. 8c), DEGs were mainly involved in the differentiation of monocytes, *T* cells, leukocytes, and phagocytosis of immune cells; the differentiation and phagocytosis of immune cells can recognize and eliminate pathogens, infected cells, and other foreign substances. The cell component (CC) class (Fig. 8d) is enriched mainly in vesicle lumens, specific granules, nuclear speckles, and Ficolin-1-rich granules; the molecular function (MF) of DEGs (Fig. 8e) regulates mainly the ability to associate with the activity of nucleoside triphosphatases (e.g., ATPase), involves the ability to bind to purine nucleotides (e.g., ATP and GTP), and involves the ability to bind to calcineurin molecules related to the ability to bind, among others.

Identification of three different gene subtypes in sepsis

To further investigate the pathogenesis, we used a consensus clustering method to categorize sepsis patients into different gene subtypes based on the 821 DEGs according to the three m6A-typed patients and named them gene subtype A, gene subtype B, and gene subtype C (Fig. 9a). In addition, we found that the differential

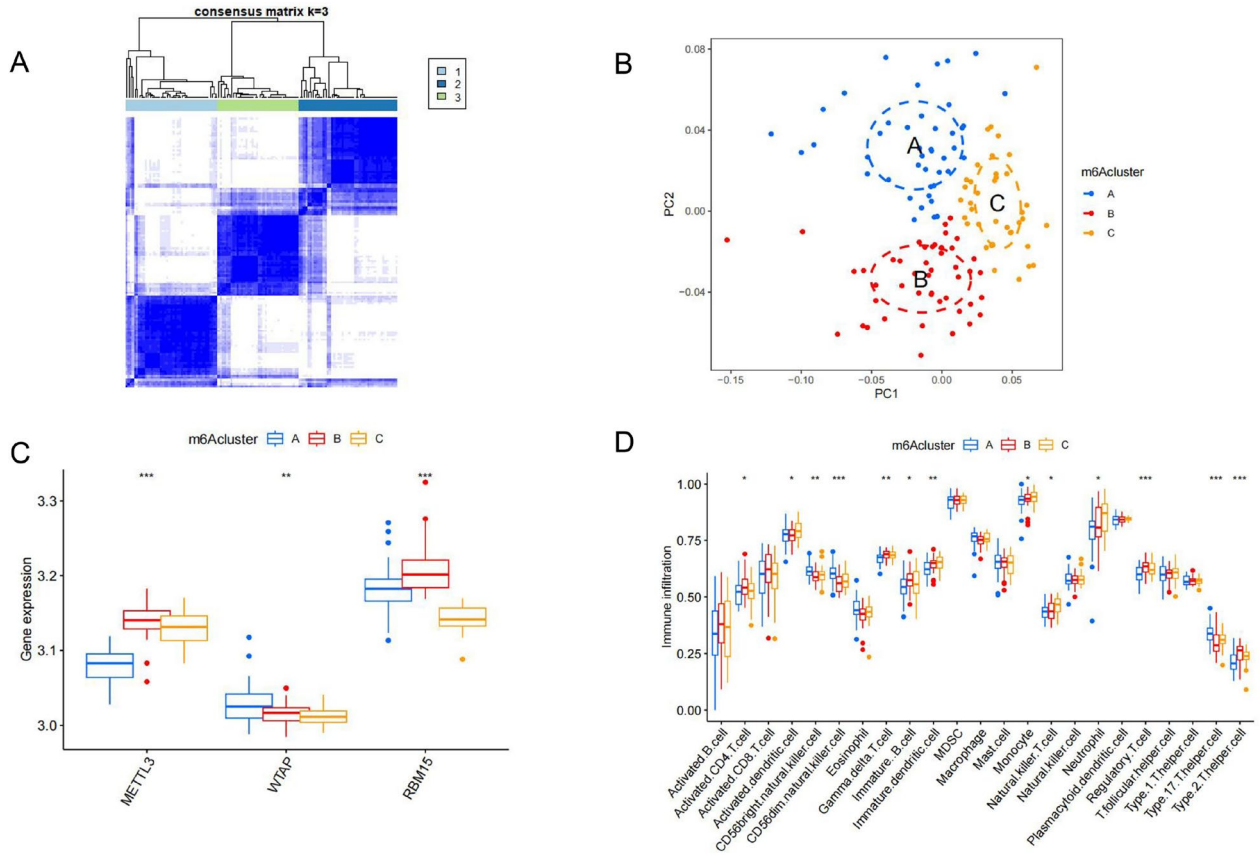

Fig. 7 Consistent clustering and immune cell analysis of three sepsis survival related genes. **A** Consistency matrix of 3 sepsis survival genes when k = 3. **B** PCA expression profiles of 3 sepsis survival genes. **C** Histograms of differential expression of 3 sepsis survival genes in the gene. **D** Differential immune cell infiltration between m6A gene cluster A and m6A gene cluster B. *means $P<0.05$, **means $P<0.01$, ***means $P<0.001$

expression levels of three sepsis survival genes and immune cell infiltration between different subtypes A, B, and C showed similar trends to the m6A typing results (Fig. 9c, d). The results again demonstrated the accuracy of delineating different subtypes. In addition, we compared two different gene scores. The results showed that the m6A scores and gene scores showed a high degree of consistency between the two in terms of trend, and the m6A scores or gene scores of subtype C were significantly higher than the high ones of subtype B (Fig. 10a, b). The relationship between the m6A subtypes, the gene subtypes, and the m6A scores was visualized in the Sankey diagram (Fig. 10c). Finally, the sepsis samples collected in our hospital were categorized into three subtypes, A, B, and C. The chi-square test allowed us to conclude that out of 127 sepsis clinical samples, subtypes A, B, and B had 20, 9, and 2 deaths, respectively (Fig. 11a); the percentage of deaths among the three subtypes was 46.5%, 19.6%, and 5.3%, respectively (Fig. 11b), with subtype A having the highest mortality rate, whereas subtype C had the lowest mortality rate, and the accuracy of the chi-square test could be concluded by Pearson chi-square and likelihood ratio (Fig. 11c).

Role of METTL3 in sepsis

Spleen flow cytometry analysis (Fig. 12a–c) showed that IL-17A expression in the three subgroups did not show statistically significant differences, while TNF-α tended to be significantly higher in the cecal ligation and puncture (CLP) + STM2457 (METTL3 inhibitor) group, and CLP was higher than that in the normal group, and there were statistically significant differences between all groups.

The results of ELISA method showed (Fig. 12d) that the expression of inflammatory factors IL-6, IL-1β and TNF-α was significantly increased in the CLP group compared with the Normal group, and the increase was more obvious in the CLP + STM2457 group, and there was a statistically significant difference between all three groups.

The HE staining of lung, liver, kidney, and small intestine tissues, as well as the pathological damage scores, are presented in Fig. 12e, f. HE staining of lung tissue showed

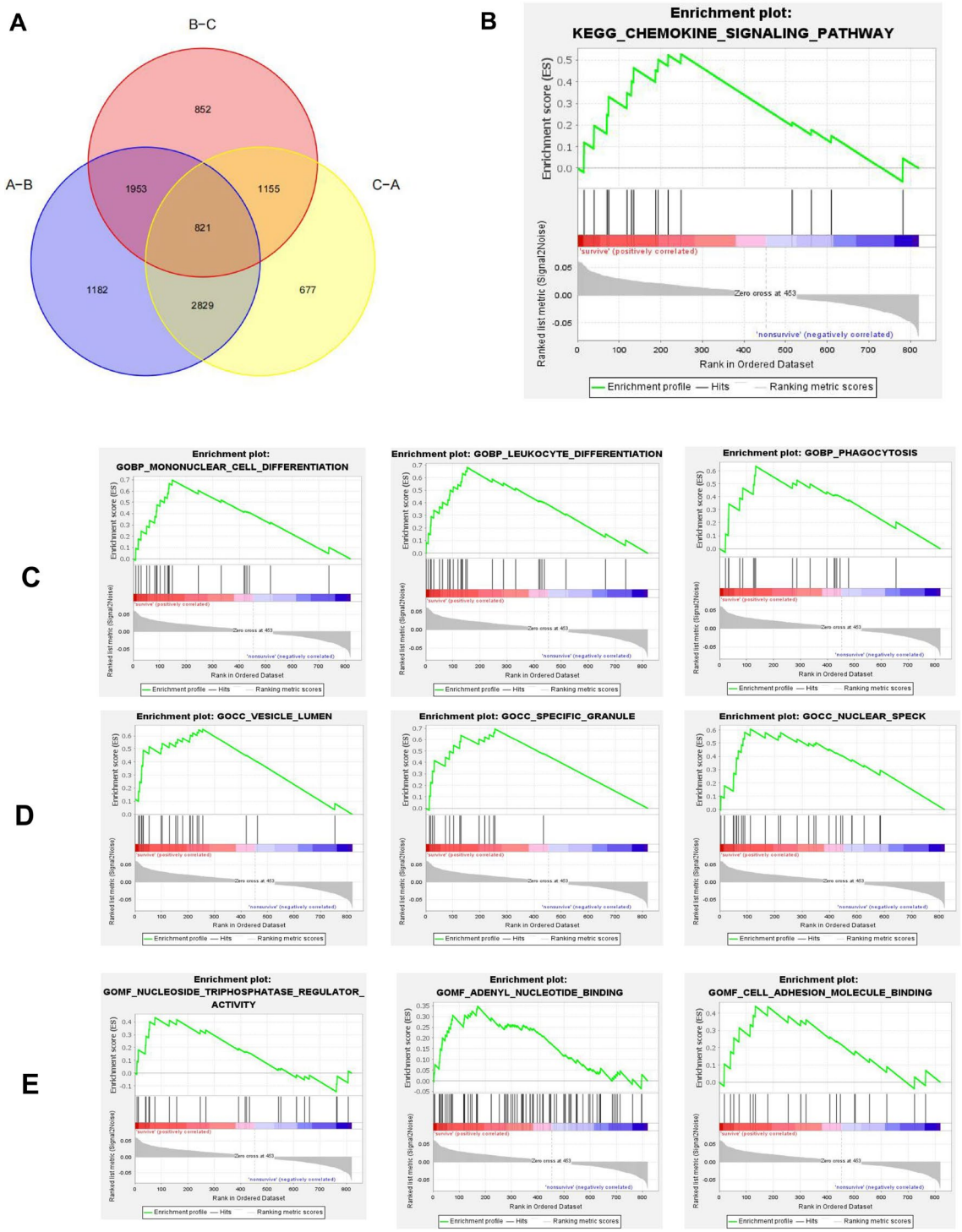

Fig. 8 Identification and functional enrichment pathways of three m6A genotyping differential genes. **A** A total of 821 DEGs were identified between subtypes A, B, and C. **B** KEGG pathway analysis of DEGs; **C** Enrichment of DEGs in the biological process (BP) category; **D** Enrichment of DEGs in the cell component (CC) category; **E** Enrichment of DEGs in molecular function (MF)

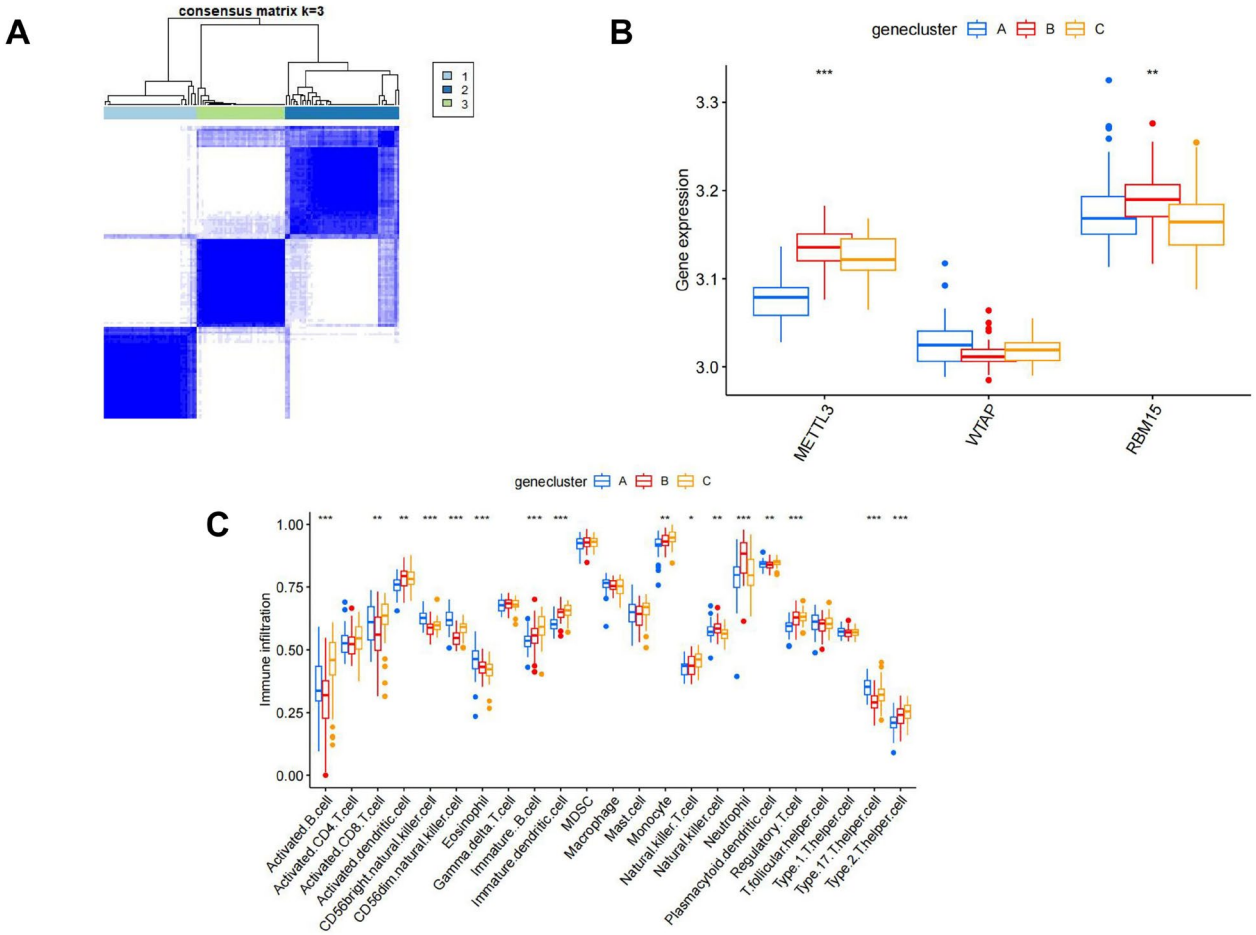

Fig. 9 Typing and analysis of 821 genes. **A** k = 3.826 DEGs genes consistency matrix. **B** Histograms of differential expression of three survival related genes in three sepsis gene subtypes. **C** The difference of immune cell infiltration among the three gene sets * means $P<0.05$, **means $P<0.01$, ***means $P<0.001$

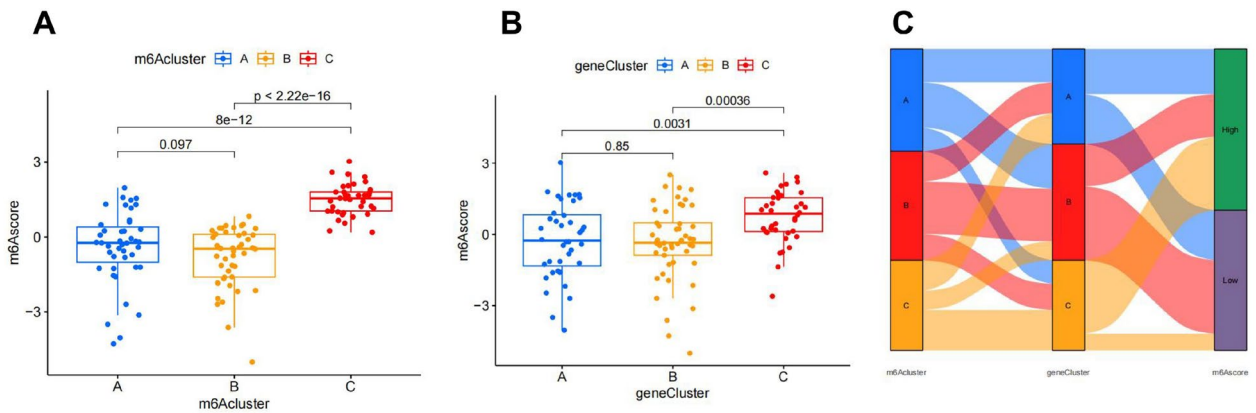

Fig. 10 **A** Comparison of m6A and genotyping: Differences in m6A scores of sepsis subtypes A, B, and C under m6A typing. **B** Differences in m6A scores of sepsis subtypes A, B and C under genotyping. **C** Scankey chart shows the relationship between m6A typing, gene typing, and m6A scoring

A

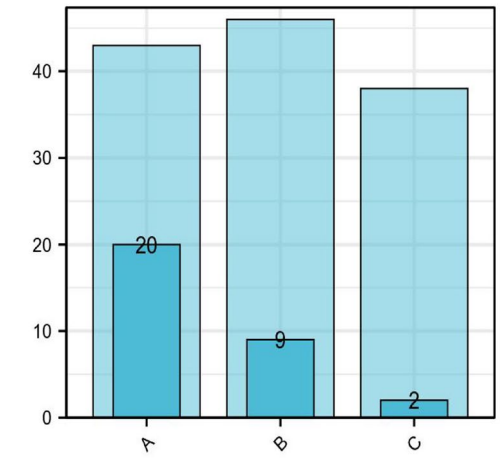

B

Ending type Cross-tabulation

			Type			
			A	B	C	Total
Ending	Non-survive	Count	20a	9b	2b	31
		Percentage by type	46.5%	19.6%	5.3%	24.4%
	Survive	Count	23a	37b	36b	96
		Percentage by type	53.5%	80.4%	94.7%	75.6%
Total		Total	43	46	38	127
		Percentage by type	100.0%	100.0%	100.0%	100.0%

C

Chi-Square Tests

	Value	Degrees of freedom	Asymptotic significance (two-sided)
Pearson chi-square	19.519a	2	.000
Likelihood Ratio	20.613	2	.000
N of Valid Cases	127		

a.(0.0%) have expected count less than 5. The minimum expected count is 9.28.

Fig. 11 Comparison of group information of sepsis patients and chi-square test results: **A** In 127 clinical samples of sepsis, the number of patients with subtype A, B and B who died; **B** proportion of patients who died in the three subtypes; **C** verification of Pearson chi-square and likelihood ratio data

(See figure on next page.)

Fig. 12 Role of METTL3 inhibitor STM2457 in CLP modeling mice. **A**, **B** Flow cytometry analysis of IL-17A and INF-γ expression differences between the three groups, **C** INF-γ was statistically different among the three groups in the histogram of cell loss results. **D** ELISA confirmed that IL-6, IL-1β, and TNF-α showed significant differences among the three groups. **E** HE staining images of lung, liver, kidney and small intestine. **F** Pathological injury score of each organ

that (Fig. 12e), normal control group: mice with clear lung tissue structure, normal alveolar size, thin alveolar wall, no obvious alveolar and interstitial edema, no hemorrhage, no inflammatory cell infiltration, and no obvious pathological changes were seen. CLP group: compared with the normal control group, the alveolar wall of the mice in the CLP group was thickened, with alveolar cavities of varying sizes, the alveolar structure was damaged, and inflammatory cell infiltration could be seen in the interstitial space. CLP + STM2457 group: mice had more pronounced alveolar wall thickening, unequal size of alveolar cavities, severe destruction of alveolar structure, and massive inflammatory cell infiltration in the interstitium. Staining of liver tissues showed that: hepatocytes around the liver sinusoids showed edema in the CLP group, and the cellular morphology was irregular, accompanied by a small amount of inflammatory cell infiltration, while the inhibition of the CLP + STM2457 group showed a more incomplete cellular structure, more pronounced edema, and more inflammatory cell infiltration. In renal tissues, a small amount of renal tubular vacuolike degeneration with a small amount of inflammatory cell infiltration was observed in the CLP group, and a large amount of renal tubular vacuolike degeneration with irregular tubular morphology and inflammatory cell infiltration was observed in the CLP + STM2457 group. In the three groups of small intestinal tissues, there was an expansion of the subepithelial space at the tip of the small intestinal villi in the CLP tissue with moderate separation of the epithelial layer from the lamina propria, and a large amount of destruction at the tip of the small intestinal villi with exposure of the capillaries in the lamina propria and infiltration of inflammatory cells was seen in the CLP + STM2457 group.

Discussion

Sepsis is a severe disease caused by systemic infection, associated with immune function, inflammatory response, and gene expression regulation [33, 34]. In this study, we identified sepsis-related m6A regulatory

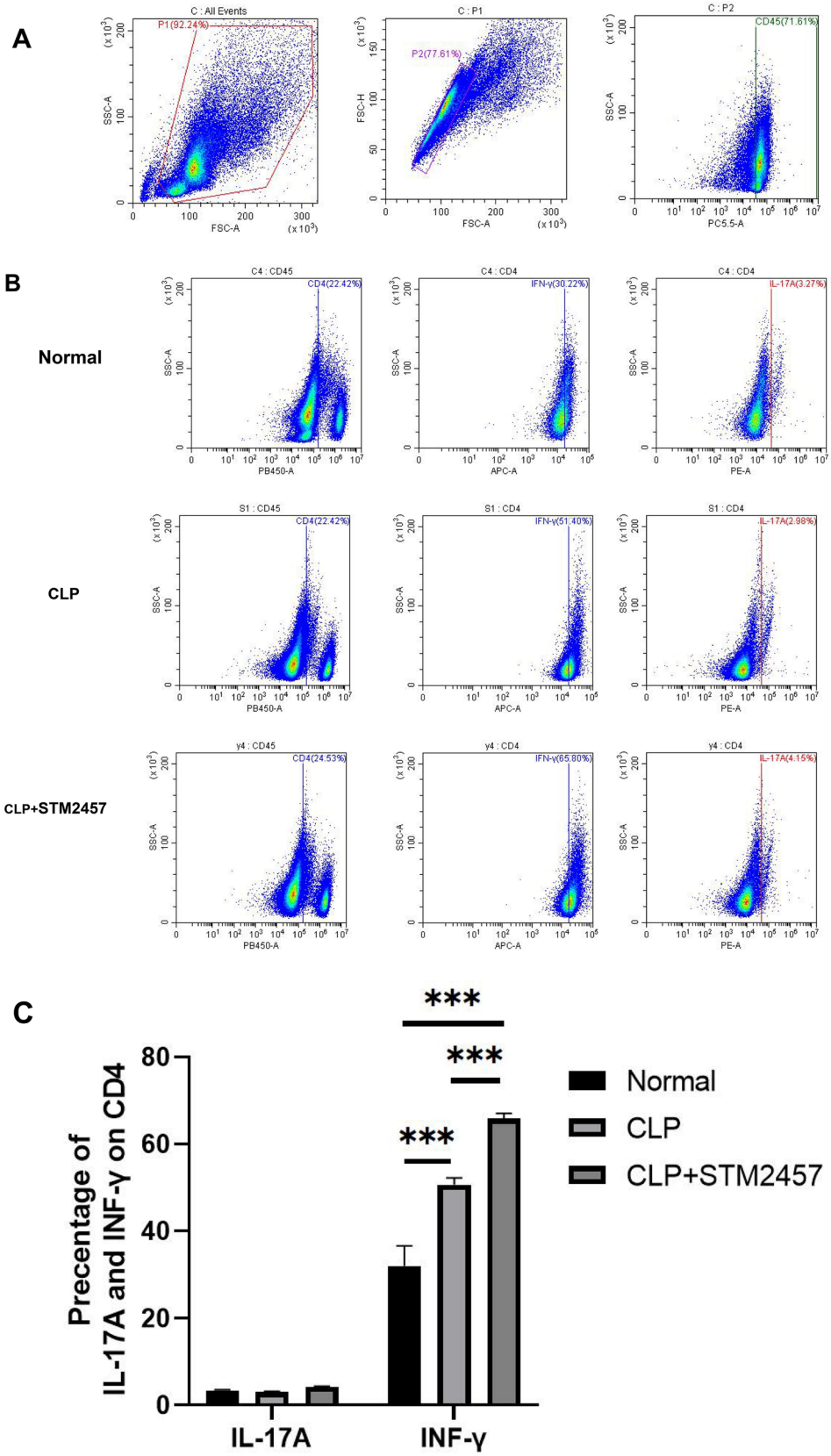

Fig. 12 (See legend on previous page.)

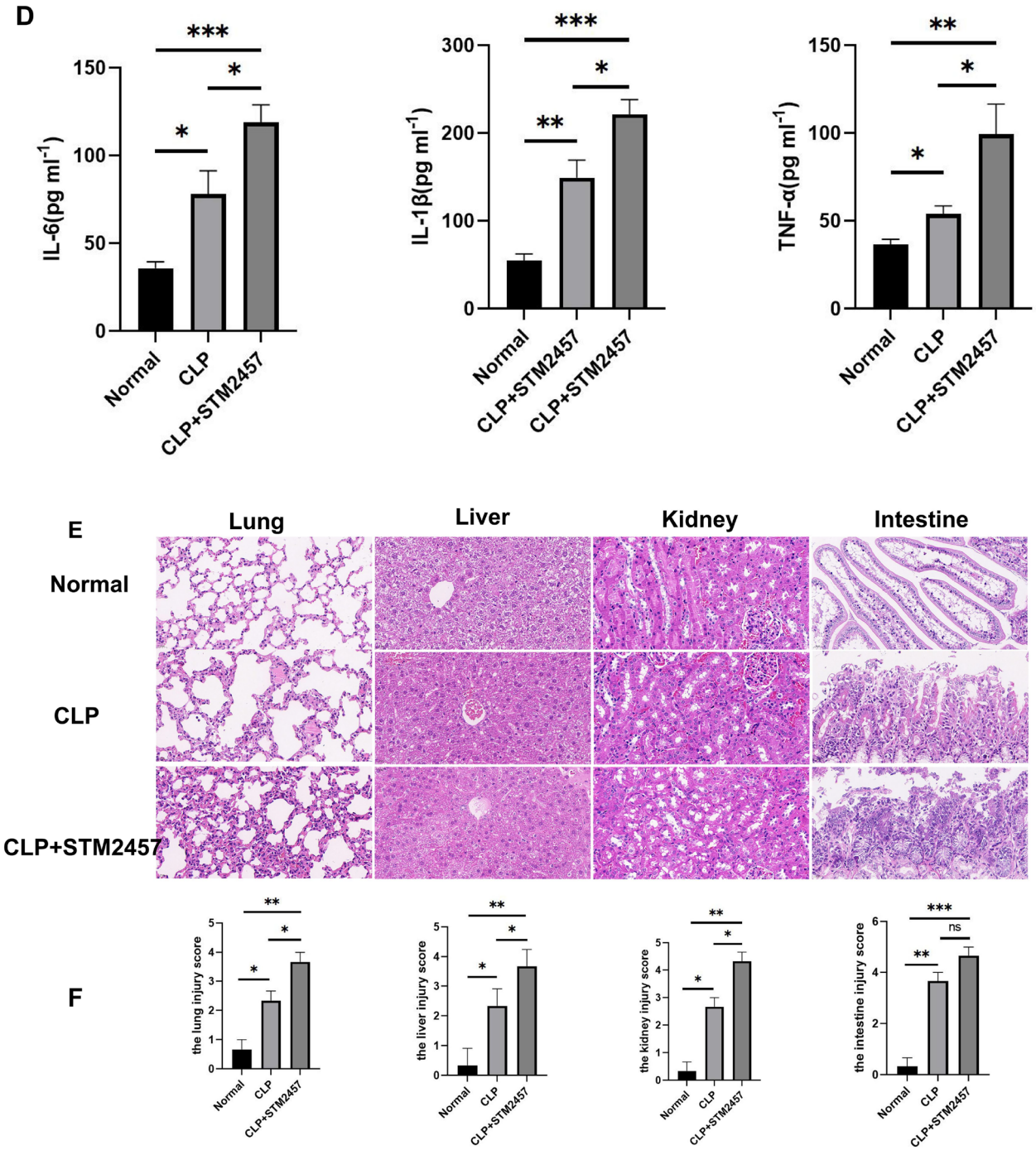

Fig. 12 continued

factors: METTL3, WTAP, and RBM15 through bioinformatics and qRT-PCR screening. The nomogram model constructed based on these three genes demonstrated high predictive accuracy. We also found that CD56 natural killer cells and Th17 were highly expressed in the death group, while neutrophils, eosinophils, and macrophages were highly expressed in the survival group. Significant differences in immune cell expression and survival outcomes among three different subtypes were observed. Animal experiments revealed that mice with early stage sepsis administered METTL3 inhibitors had a higher mortality rate.

Initially, we extracted the expression levels of 26 methylated genes from data set GSE54514, using RF, SVM–RFE, and LASSO methods to filter out four differentially expressed genes. The significant correlation of METTL3, WTAP, and RBM15 with sepsis was verified through qRT-PCR.

METTL3 (methyltransferase-like protein 3) is an RNA methyltransferase, whose primary function is to add methyl groups to mRNA, thereby regulating gene expression [35, 36]. The function of METTL3 in inflammatory activity was further explored by researchers. It was elucidated that METTL3-mediated m6A methylation promotes neutrophil activation via modification of TLR4 mRNA and then activates its translation and slows its degradation in lipopolysaccharide (LPS)-induced endotoxemia [37]. WTAP (Wilms' tumor associated protein) is an RNA methyltransferase that plays a role in apoptosis and cell cycle control [38]. Previous research indicated that WTAP directly affects the release of inflammatory mediators such as TNF-α and IL-6, and its increased level is closely related to the exacerbation of inflammatory response. Its knockout or inhibition may effectively alleviate inflammatory response [39]. The main function of RBM15 (RNA binding motif protein 15) is to participate in RNA splicing, maturation, and stability regulation. In a study on an Alzheimer's disease mouse model targeting miRNA-155/TNFSF10 to inhibit inflammation in the retina, RBM15 may play an important role [40]. In brief, METTL3, WTAP, and RBM15 are of great importance in regulating inflammatory responses and immune functions, and are closely related to the progression of inflammation. Therefore, we hypothesize that these three genes may also play an essectial part in the development and progression in sepsis.

Based on the three key genes identified, we constructed a nomogram model to predict the outcome of sepsis. After analysis, the AUC value of the model was 0.883, and the AUC value of the validation model reached 0.985, confirming the generalizability of model. In addition, the results of the model's calibration curve, decision curve, and clinical impact curve indicated that this prediction model has high accuracy. This model not only provides clinicians with a powerful prognostic tool, but also helps identify high-risk patients earlier, enabling more aggressive interventions and offering personalized treatment plans for patients.

Sepsis patients with different proportions of immune cells turned out with different prognoses. It was found that CD56dim natural killer cells and Th17 were highly expressed in patients with a fatal outcome. CD56dim natural killer cells are a subset of NK cells with strong cytotoxic activity. Researchers have discovered that in sepsis patients, the Researchers of T lymphocytes significantly decreased, while the proportion of NK lymphocytes significantly increases [41, 42]. Zhang and colleagues found that autophagy within the body can attenuate Th1 and Th17 responses, thereby preventing sepsis induced by methicillin-resistant *Staphylococcus aureus* (MRSA) [43]. Underexpression of neutrophils, eosinophils, and macrophages was also observed in patients with a fatal outcome, was also observed that immunosuppression occurred within these patients [44]. An earlier article reported consistent conclusions as in the present study, implying that the immunosuppression in sepsis can be significantly alleviated by enhanced expression of Spns2/S1P in macrophages [45]. The decreased level of immune cells in patients with sepsis indicated that these m6A methylated genes may be key targets leading to immune suppression. Clinically, intervening in the expression of these genes can improve the patient's immune status and reduce mortality.

Using consensus clustering based on the similarity of m6A modulator expression levels, we found that when $k=3$, the clustering had the best stability, dividing sepsis patients into three subtypes. Significant differences were observed in the expression of immune cells such as CD56dim, CD56bright natural killer cells, and Th17 among different subtypes, implying that different subtypes exhibit different immune states. Further analysis revealed that in subtype A, the expression of Treg, monocytes, NK cells CD4+, and other cells was significantly lower compared to groups B and C, suggesting that patients in subtype A may experience immunosuppression, resulting in a higher mortality rate. Conversely, in patients of subtype C, the expression of immune cells was higher than in subtype B patients, indicating a lower occurrence of immunosuppression in the subtype C group. Chi-square tests was conducted on the clinical samples and the result showed significant differences in survival rates among the three classifications. The proportion of patients with a fatal outcome in subtype C samples was only 5.3%, significantly lower than types A and B.

In this study, we performed pathway and functional enrichment analysis on 821 differentially expressed genes (DEGs) among the three subtypes. KEGG enrichment analysis results showed that DEGs were mainly enriched in the chemokine signaling pathway. Previous studies have found higher expression levels of chemokines in severe COVID-19 patients developing sepsis [46], highlighting the important role of chemokines in the progression of sepsis.

To better validate the accuracy of m6A typing, we conducted gene subtype classification through consensus clustering among 821 DEGs across the three subtypes. We observed that when $k=3$, the clustering had the best

stability, making it most appropriate to divide them into three types. By comparing with the m6A typing at the immune cell level and in terms of PCA scores, we discovered that the trends in immune cell expression among the three subtypes in the m6A typing and gene typing were very similar, confirming the accuracy of the m6A typing. In addition, by calculating m6A scores through PCA analysis to quantify m6A subtypes, we found that both typing methods indicated that subtype C had higher scores, while the scores in types A and B had no statistical differences. This suggests that in this model, subtypes with higher m6A scores are less likely to experience immunosuppression, resulting in higher patient survival rates.

These immune analyses indicated that m6A methylated genes may influence the immune function of patients via regulation the expression of neutrophils, macrophages, and Th17 cells, leading to worsened conditions in sepsis patients. In addition, the outcomes differed between sepsis subtypes based on the expression levels of these m6A methylated genes. Future research should focus on developing small-molecule inhibitors or agonists targeting these genes to regulate immune responses and inflammation processes.

Previous studies have reported that endotoxins or viral infections upregulate the level of HIF-1α in DCs through the CXCR1 and ERK signaling pathways, stimulating the differentiation of CD4+T cells into Th1 and Th17, thereby promoting disease progression [47]. TNF-α is primarily secreted by immune cell Th1, and IL-17A is mainly secreted by immune cell Th17. In our CLP model, splenic cell flow cytometry analysis of TNF-α and IL-17A revealed increased expression levels of TNF-α in sepsis, and inhibition of METTL3 resulted in higher expression levels of TNF-α; however, there was no significant difference in the expression of IL-17A among the three groups. This suggested that Th1 cells could play an important role in sepsis and that the METTL3 inhibitor STM2457 may regulate the progression of the disease by modulating Th1 cells, which is consistent with significant higher level of Th1 cells in patients with sepsis [48]. Previous studies have shown that the inflammatory cytokines IL-6, IL-1β, and TNF-α were significantly elevated during the inflammatory response phase of the body [49]. Our serum enzyme-linked immunosorbent assay results showed a significant higher expression level of these three inflammatory cytokines in septic mice and even higher levels when inhibiting METTL3, indicating that inhibition of METTL3 could trigger a more severe inflammatory activity. Organ damage scores from HE staining showed more severe multi-organ (lung, liver, kidney, and intestine) damage in CLP-induced septic mice and the organ injury was higher in METTL3-inhibited CLP-mice group. In short, severe inflammatory responses and organ damage were observed in septic mice and both were more significant with METTL3 inhibition. Significant higher expression of Th1 cells after METTL3 inhibition triggered a stronger inflammatory response and multi-organ dysfunction, ultimately resulting in a higher mortality rate in sepsis patients.

However, this study still has some limitations. First, the small number of clinical samples from septic patients we collected might introduce bias into the results. In addition, the unequal sample sizes between different outcome groups could render the differential expression analysis results meaningless or lead to false positives. Currently, the indicators in our prognostic model are limited to gene expression. In the future, we can add more clinical details to the nomogram. Although we have found that m6A methylation may affect prognosis by influencing the body's immune function, its specific mechanisms and pathways still need further study.

Conclusions

In this study, the m6A methylated genes METTL3, WTAP, and RBM15 were identified in sepsis. An accurate survival model was established, which revealed a lower probability of immunosuppression and a higher survival rate for the high m6A scoring isoforms compared to the other two m6A isoforms. It was also found that immune homeostasis is crucial in sepsis development and influences clinical outcomes. Furthermore, the study demonstrated that inhibition of the METTL3 gene could worsen multi-organ functional damage in sepsis. This research provides new insights into potential biomarkers and personalized treatment strategies for sepsis management.

Supplementary Information

The online version contains supplementary material available at https://doi.org/10.1186/s40001-024-02194-8.

Additional file 1
Additional file 2
Additional file 3
Additional file 4
Additional file 5

Acknowledgements
The authors are grateful for the availability of data sets through GEO project, XIANTAO platform, and other groups.

Author contributions
Shaokang Wang, Zhonghua Lu, Na Cheng and Yun Sun participated in the screening and assembly of the data set, the analysis and interpretation of the data, and wrote the main manuscript text. Siye Shen, Daiyun Liang and Wenjun Zhou participated in the topic discussion and data statistical analysis. Shaokang Wang, Siye Shen, Daiyun Liang Lijun Cao and Pinjie Zhang participated in animal experiment. Weili Yu, Zhonghua Lu and Na Cheng contributed

to the R statistical analysis of the study. All authors participated in the experiment and drafted the manuscript together.

Funding
This study was supported by Provincial Quality Engineering Project of Higher Education Institutions of Anhui Province (2022jyxm750), Natural Science Research Project of Anhui Higher Education Institutions (2023AH053168) and Anhui Province Traditional Chinese Medicine Inheritance and Innovation Research Project (2024CCCX128).

Availability of data and materials
No datasets were generated or analysed during the current study.

Declarations

Institutional review board statement
This study was approved by the Animal Care and Use Committee of Anhui Medical University (Ethics Committee Approval Number: LLSC20200404).

Consent for publication
Not applicable.

Competing interests
The authors declare no competing interests.

Received: 28 September 2024 Accepted: 2 December 2024
Published online: 19 December 2024

References

1. Liang X, et al. Risk factors and outcomes of urosepsis in patients with calculous pyonephrosis receiving surgical intervention: a single-center retrospective study. BMC Anesthesiol. 2019;19(1):61.
2. Oczkowski S, et al. Surviving Sepsis Campaign Guidelines 2021: highlights for the practicing clinician. Pol Arch Intern Med. 2022;132(7–8):16290–16290.
3. Plesa-Furda P, et al. Abdominal sepsis-current definitions and practice. Chirurgia (Bucur). 2021;116(6 Suppl):S16–27.
4. Liu D, et al. Sepsis-induced immunosuppression: mechanisms, diagnosis and current treatment options. Mil Med Res. 2022;9(1):56.
5. Sygitowicz G, Sitkiewicz D. Molecular mechanisms of organ damage in sepsis: an overview. Braz J Infect Dis. 2020;24(6):552–60.
6. Jiang X, et al. The role of m6A modification in the biological functions and diseases. Signal Transduct Target Ther. 2021;6(1):74.
7. He PC, He C. m6A RNA methylation: from mechanisms to therapeutic potential. EMBO J. 2021;40(3): e105977.
8. Wang W, Wang H, Sun T. N6-methyladenosine modification: regulatory mechanisms and therapeutic potential in sepsis. Biomed Pharmacother. 2023;168(40): 115719.
9. Wan W, et al. METTL3/IGF2BP3 axis inhibits tumor immune surveillance by upregulating N(6)-methyladenosine modification of PD-L1 mRNA in breast cancer. Mol Cancer. 2022;21(1):60.
10. Huang H, et al. Altered Expression of the m6A Methyltransferase METTL3 in Alzheimer's Disease. eNeuro. 2020;7(5):1.
11. Geng Q, et al. Diagnostic gene signatures and aberrant pathway activation based on m6A methylation regulators in rheumatoid arthritis. Front Immunol. 2022;13:1041284.
12. He L, et al. Functions of N6-methyladenosine and its role in cancer. Mol Cancer. 2019;18(1):176.
13. Zhang H, et al. Neutrophil extracellular traps mediate m6A modification and regulates sepsis-associated acute lung injury by activating ferroptosis in alveolar epithelial cells. Int J Biol Sci. 2022;18(8):3337–4335.
14. Liang L, et al. m6A-mediated upregulation of miRNA-193a aggravates cardiomyocyte apoptosis and inflammatory response in sepsis-induced cardiomyopathy via the METTL3/miRNA-193a/BCL2L2 pathway. Exp Cell Res. 2023;430(1): 113712.
15. Kim KS, et al. Immune gene expression networks in sepsis: a network biology approach. PLoS ONE. 2021;16(3): e0247669.
16. Li F, et al. Diagnostic, clustering, and immune cell infiltration analysis of m6A regulators in patients with sepsis. Sci Reports. 2023;13(1):2532.
17. Youssef AAA. Global-local least-squares support vector machine (GLocal-LS-SVM). PLoS ONE. 2023;18(4): e0285131.
18. Wong A, et al. Using LASSO regression to estimate the population-level impact of pneumococcal conjugate vaccines. Am J Epidemiol. 2023;192(7):1166–80.
19. Strobl C, et al. Bias in random forest variable importance measures: illustrations, sources and a solution. BMC Bioinformatics. 2007;8(6):25.
20. Toth R, et al. Random forest-based modelling to detect biomarkers for prostate cancer progression. Clin Epigenetics. 2019;11(1):148.
21. Friedman J, Hastie T, Tibshirani R. Regularization paths for generalized linear models via coordinate descent. J Stat Softw. 2010;33(1):1–22.
22. Yu P, et al. Extrathyroidal extension prediction of papillary thyroid cancer with computed tomography based radiomics nomogram: a multicenter study. Front Endocrinol (Lausanne). 2022;13: 874396.
23. Vickers AJ, Elkin EB. Decision curve analysis: a novel method for evaluating prediction models. Med Decis Making. 2006;26(6):565–74.
24. Tanzhu G, et al. Molecular subtypes and prognostic signature of pyroptosis-Related lncRNAs in glioma patients. Front Oncol. 2022;12: 779168.
25. Wang L, et al. Identification of distinct clinical phenotypes of cardiogenic shock using machine learning consensus clustering approach. BMC Cardiovasc Disord. 2023;23(1):426.
26. Hanzelmann S, Castelo R, Guinney J. GSVA: gene set variation analysis for microarray and RNA-seq data. BMC Bioinformatics. 2013;14:7.
27. Charoentong P, et al. Pan-cancer immunogenomic analyses reveal genotype-immunophenotype relationships and predictors of response to checkpoint blockade. Cell Rep. 2017;18(1):248–62.
28. Modesto IAV, Aguar CM, Medina VA. Clinical implications of the rheological theory in the prevention of ventilator-induced lung injury. Is mechanical power the solution? Med Intensiva (Engl Ed). 2019;43(6):373–81.
29. Zhao T, et al. Activation of c-Src tyrosine kinase mediated the degradation of occludin in ventilator-induced lung injury. Respir Res. 2014;15(1):158.
30. Liang H, et al. Metformin attenuated sepsis-related liver injury by modulating gut microbiota. Emerg Microb Infect. 2022;11(1):815–28.
31. Tan C, et al. Inhibition of aerobic glycolysis alleviates sepsis-induced acute kidney injury by promoting lactate/Sirtuin 3/AMPK-regulated autophagy. Int J Mol Med. 2021;47(3):1–1.
32. Sun S, et al. Neutrophil extracellular traps impair intestinal barrier functions in sepsis by regulating TLR9-mediated endoplasmic reticulum stress pathway. Cell Death Dis. 2021;12(6):606.
33. Mirijello A, Tosoni A. New strategies for treatment of sepsis. Medicina. 2020;56(10):527.
34. Salomao R, et al. Sepsis: evolving concepts and challenges. Braz J Med Biol Res. 2019;52(4): e8595.
35. Chen L, Zhang C, Ma W, Huang J, Zhao Y, Liu H. METTL3-mediated m6A modification stabilizes TERRA and maintains telomere stability. Nucleic Acids Res. 2022;50(20):11619–34. https://doi.org/10.1093/nar/gkac1027. (**PMID:36399511;PMCID:PMC9723618**).
36. Xu Y, et al. METTL3 promotes lung adenocarcinoma tumor growth and inhibits ferroptosis by stabilizing SLC7A11 m6A modification. Cancer Cell Int. 2022;22(1):1–11.
37. Luo S, et al. METTL3-mediated m6A mRNA methylation regulates neutrophil activation through targeting TLR4 signaling. Cell Rep. 2023;42(3): 112259.
38. Lan J, et al. WTAP-mediated N (6)-methyladenosine modification of NLRP3 mRNA in kidney injury of diabetic nephropathy. Cell Mol Biol Lett. 2022;27(1):51.
39. Han X, et al. RNA m (6)A methylation modulates airway inflammation in allergic asthma via PTX3-dependent macrophage homeostasis. Nat Commun. 2023;14(1):7328.
40. Burgaletto C, et al. Targeting the miRNA-155/TNFSF10 network restrains inflammatory response in the retina in a mouse model of Alzheimer's disease. Cell Death Dis. 2021;12(10):905–905.
41. Bacarea A, et al. Immune profile of patients-a new approach in management of sepsis and septic shock? Exp Ther Med. 2024;27(5):203.
42. Uchida T, Seki S, Oda T. Infections, Reactions of Natural Killer T Cells and Natural Killer Cells, and Kidney Injury. Int J Mol Sci. 2022;23(1):479.

43. Zhang S, et al. The attenuation of Th1 and Th17 responses via autophagy protects against methicillin-resistant Staphylococcus aureus-induced sepsis. Microbes Infect. 2021;23(8): 104833.
44. Scott J, et al. Role of immunosuppression in an antibiotic stewardship intervention and its association with clinical outcomes and antibiotic use: protocol for an observational study (RISC-sepsis). BMJ Open. 2022;12(12): e068321.
45. Fang C, et al. Enhancing Spns2/S1P in macrophages alleviates hyper-inflammation and prevents immunosuppression in sepsis. EMBO Rep. 2023;24(8): e56635.
46. Kocak Tufan Z, Kayaaslan B, Mer M. COVID-19 and Sepsis. Turkish J Med Sci. 2021;51(1):3301–11.
47. Zhuang W, et al. CXCR1 drives the pathogenesis of EAE and ARDS via boosting dendritic cells-dependent inflammation. Cell Death Dis. 2023;14(9):608.
48. Liu Y, Wang X, Yu L. Th17, rather than Th1 cell proportion, is closely correlated with elevated disease severity, higher inflammation level, and worse prognosis in sepsis patients. J Clin Lab Anal. 2021;35(5): e23753.
49. Tan F, et al. Diabetes exacerbated sepsis-induced intestinal injury by promoting M1 macrophage polarization via miR-3061/Snail1 signaling. Front Immunol. 2022;13: 922614.

Publisher's Note